Elastic deformation of helical-conical boron nitride nanotubes

F. F. Xu, Y. Bando, D. Golberg, R. Z. Ma, Y. B. Li, and C. C. Tang

Citation: The Journal of Chemical Physics **119**, 3436 (2003); doi: 10.1063/1.1589738
View online: http://dx.doi.org/10.1063/1.1589738
View Table of Contents: http://scitation.aip.org/content/aip/journal/jcp/119/6?ver=pdfcov
Published by the AIP Publishing

Elastic deformation of helical-conical boron nitride nanotubes

F. F. Xu,[a] Y. Bando, D. Golberg, R. Z. Ma, Y. B. Li, and C. C. Tang
Advanced Materials Laboratory, National Institute for Materials Science, Namiki 1-1, Tsukuba, Ibaraki 305-0044, Japan

(Received 28 January 2003; accepted 15 May 2003)

Boron nitride nanotubes with hollow conical-helix geometry have exhibited striking flexibility and elasticity comparable to metals. During an electron-beam induced deformation at room temperature, the nanotubes can be bent by a maximum angle as high as 180° and then retrieve the starting morphology without any evidence of structural failure. The outstanding low-temperature elasticity in this nano-material is interpreted by a theoretical model, displaying deformation processes dominated by slide of filaments along with changes in apex angles stepwise. The specific tubular geometry is believed to take advantages of both high stiffness and extraordinary flexibility of BN filaments, and easiness of interlayer slide in graphitic structure, hence leading to high resistance to fracture. © *2003 American Institute of Physics.* [DOI: 10.1063/1.1589738]

I. INTRODUCTION

Carbon nanotubes (CNTs) consist of curved filaments displaying a cylindrical morphology.[1] The arrangement of hexagon network relative to the tube axis may vary, leading to different tubular configurations, namely armchair, zigzag, or chiral nanotubes. Experiments and theoretical calculations have pointed out that CNTs have the largest know stiffness along the axial direction and bending flexibility.[2–14] They can sustain large strains without evidence of collapse or failure. Molecular dynamics simulation of deformation illustrates a bond-rotation defect by the accumulation of elastic stress.[15–18] For example, an armchair nanotube in tension that is beyond a critical value releases its excess strain via spontaneous formation of double pentagon–heptagon defect pairs.[18]

Graphite-like boron nitride (BN) is a structural analog of graphite but exhibits distinguishing features including high chemical and thermal stability, and a wide-band-gap insulating ($E_b \sim 5.5$ eV) property.[19–22] These characteristics may be important for some specific applications, especially at the nanoscale level. BN nanotubes have been found, by both experiments and theoretical calculations, to be the stiffest insulating materials since their Young's modulus (1.1–1.3 TPa) is approaching that of CNTs (1.3–1.8 TPa).[6–8,23,24] Since BN nanotubes and CNTs are isoelectronic, a similar failure mechanism in response to a large tension has been expected. Simulation has also indicated formation of 5|7|7|5 dislocation dipoles in spite of its homoelemental B–B and N–N bonds. Compared to CNTs, formation energy of the primary defect is higher and remains positive at larger strain in BN nanotubes, thus suggesting greater yield resistance.[25]

Despite the above remarkable mechanical properties, graphitic cylindrical nanotubes inevitably exhibit some shortcomings, which limits their forthcoming applications. One is that the properties are highly structural dependent. They could be either plastic or brittle, depending on the external conditions and tube symmetry.[16–18] So far, a critical control of tube symmetry in the synthesis is still not available. Another disadvantage is that all CNTs are brittle at high strain and low temperature.[17] Development of low-temperature flexible inorganic nanomaterial is of great significance and presently highly demanded. Recently, we observed a new tubular form of graphite-like BN, showing a specific hollow conical-helix (HCH) geometry.[26] It will be seen in the present study that such helical-conical nanotubes (HCNTs) exhibit striking flexibility and elasticity comparable to metals. HCNTs forbear extremely high strain even at room temperature without any evidence of fracture. The outstanding low-temperature elasticity stems from two prerequisite structural elements, i.e., hollow conical-helix geometry and nanoscale. Here, electron-beam induced deformation of BN HCNTs under a transmission electron microscope (TEM) is reported. A new deformation model is established, where no topological dislocations are necessary to be created in order to release large strains. The nanotubes keep the rigid honeycomb filamentary configuration during the deformation with a sole change in apex angles.

II. EXPERIMENTAL METHODS

BN HCNTs were synthesized by employing a substitution reaction from CNTs by B_2O_3 in N_2 atmosphere. A postheating process at an increased temperature is undertaken. The main experimental parameters that have been found to determine the structures of the final products are the starting compositions and heating/postheating temperatures. HCNTs were only observed in specimens heated at 1700 °C and postheated at temperatures over 1750 °C with the starting B_2O_3/CNT ratio larger than 8:1. Details of synthesis, structure, and formation mechanism will be reported elsewhere.[26]

The x-ray diffraction (XRD) data were collected by a powder diffractometer (Rigaku Rint 2000S) with graphite-monochromatized Cu$K\alpha$ radiation ($\lambda = 0.15405$ nm).

[a]Author to whom correspondence should be addressed; electronic mail: xu.fangfang@nims.go.jp

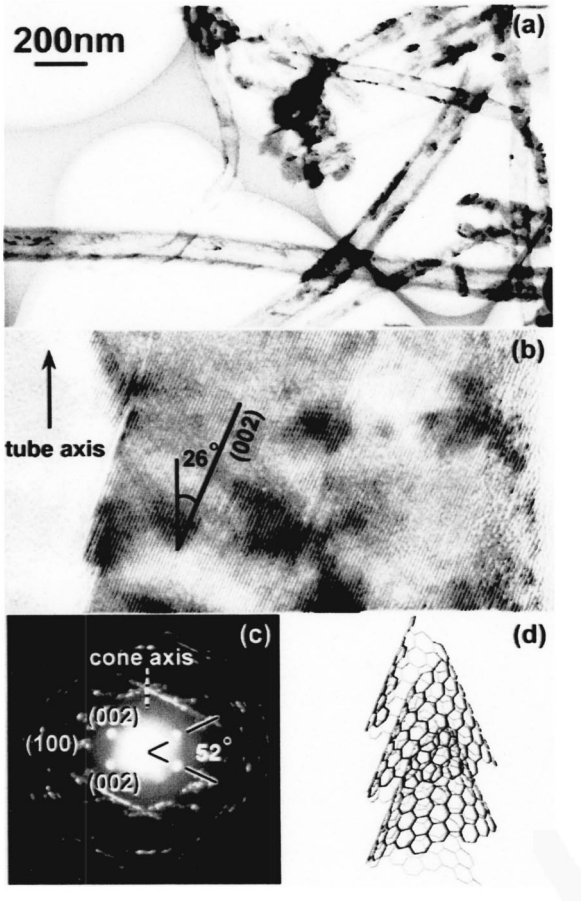

FIG. 1. Structure and morphology of BN HCNTs. (a) TEM bright-field image; (b) lattice image of the sidewall of a nanotube; (c) typical electron diffraction pattern; (d) structural model.

Electron-beam induced deformation of nanotubes was performed in a 300 kV field-emission transmission electron microscope (JEOL-3000F) at room temperature. This allows *in situ* observation of deformation process.

III. RESULTS

Our recent work[26] has indicated that BN HCNT consists of a single narrow filamentary belt wrapping helically and conically, showing continuous interior tunnels and geometry of Archimedes spiral as shown in Fig. 1. This is confirmed by XRD and electron energy-loss spectra which indicate a pure graphite-like BN phase with the lattice parameters of $a=0.2502$ nm and $c=0.3333$ nm; and lattice image [Fig. 1(b)] and diffraction pattern [Fig. 1(c)] which are in good agreement with the reported conical geometry.[27–32] Helical wrapping rather than stacking of monolayer cones is concluded from the fact that majority of the observed disclination configurations contain an overlap angle in addition to $n60°$.[26] For a helical cone, basal cones stack on top of one another, but interconnect in a helical fashion by a single screw dislocation along the axis of the conical fiber [see the structural model in Fig. 1(d)]. The helical cones have been found to have well-defined apex angles (θ_{apex}) and hence disclination angles (θ_D), which were ascribed to high densities of coincidence lattice sites between overlapping layers.[27–29] In general, disclination angles that lead to coincidence configuration include multiples of 60° and their combination with additional overlap angles of, e.g., 13.2°, 21.8°, and 27.8°.[27–32]

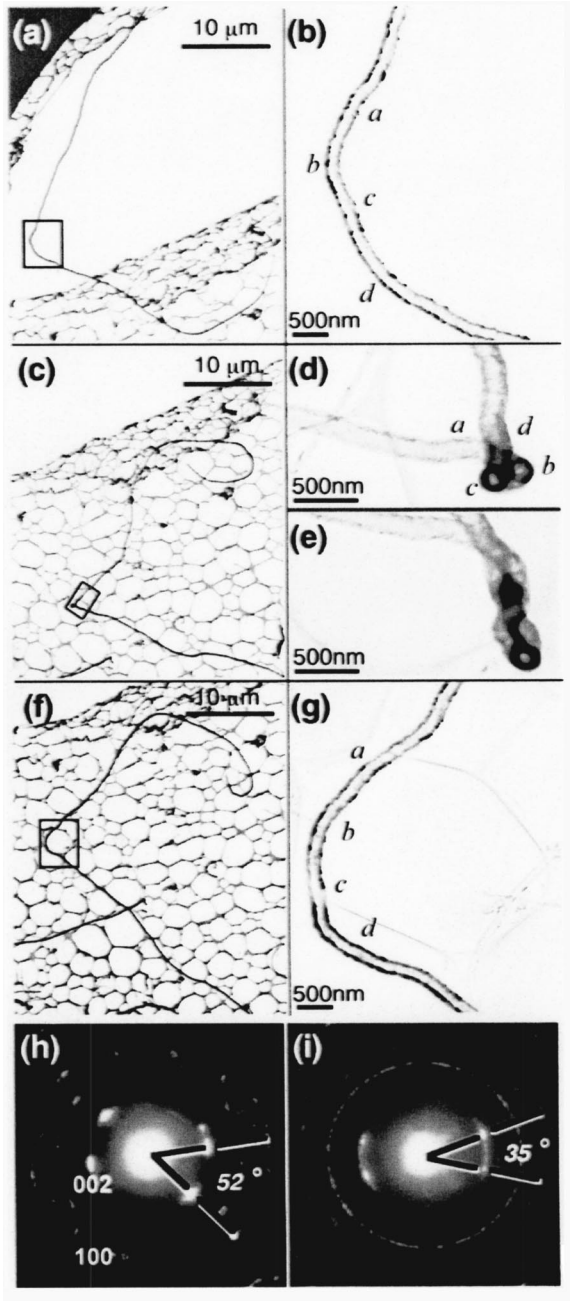

FIG. 2. TEM image of an individual BN HCNT bearing deformation through changing the electron beam intensity (see the text).

The specific geometry of HCNTs has brought about a fascinating deformation behavior, as has been observed directly under *in situ* transmission electron microscopy. Figure 2(a) shows a wavy BN HCNT residing on a copper grid. The framed region in Fig. 2(a) is enlarged in Fig. 2(b). Here, we focus on this corner region and keep on showing it in Figs. 2(d), 2(e), and 2(g), since this part will bear the most severe deformation during the succeeding electron illumination with frequently changed intensity. By monitoring *a*, *b*, *c*, and *d*

sites on the nanotube, the change in shape during deformation can easily be recognized.

As soon as the current density is rapidly increased from 90 to 160 pA/cm^2 via focusing the incident beam, the nanotube jumps over onto the foil and shows unpredictable modification of its bent morphology with increased curvature [Fig. 2(c)]. The bending behavior of BN HCNT via changing the electron beam intensity could be due to either electrostatic forces or charging effects in insulating materials.[33] The corner region is now kinked as indicated by the marks *a, b, c*, and *d*, showing *two* close-packed cross sections of the tubule. Since the nanotube and the kink can be focused with a deviation in defocus values of ~20 nm, the erected kink involves a small depth, indicative of an abrupt change of the tubule orientation. Thus, an extremely large curvature (~0.007 nm^{-1}) is present at the kink tip. The HCNT has been bent by at least 180°. Slight shift of electron beam in a certain direction will enhance twisting of kink area [Fig. 2(e)]. By shifting the electron beam back, the image of Fig. 2(d) is retrieved. When the beam intensity is reduced (back to ~90 pA/cm^2), the tube finally reverts to the morphology similar to that shown in Fig. 2(a) without any evidence of structural failure, hence exhibiting a spring-like behavior. Though similar spring-like phenomenon was also observed in CNTs, the present HCNTs have apparently been subject to the largest strain and torsion ever observed in nanotubes[33–35] and inorganic materials.

IV. DEFORMATION MODELS

Though graphite-like BN is brittle, BN HCNT has exhibited remarkable elastic behavior under deformation. It has been known that the shear modulus of graphite (4.5 GPa) is smaller than its Young's modulus (1 TPa). Therefore, it is much easier to slide the filaments than break them.[34,35] The weakened interaction forces between the neighboring filaments in HCNTs due to the poor crystallinity [since the smallest Σ7 CSL (coincidence site lattice) is still $\sqrt{7}$ times larger than *h*-BN unit cell[27–29,36]] normal to the sheet plane further favor sliding under external stress. It will be seen that no topological defects are necessary to be introduced during the deformation of HCNTs, which is on the other hand solely determined by the crystallographic factors since only rotation and/or slide of filaments are involved in the deformation owing to the specific geometry of HCNTs. This is due to the fact that bending, stretching, twisting and even, a compressive stress normal to the tube axis contain a shear along certain cone surfaces. Here, a deformation model is established for HCNT, which can interpret any kind of deformation process in hollow conical-helix.

The filamentary fragment framed by *ABCD* in Fig. 3 can wrap to form HCNT with the disclination angle of 360°-$\angle AOB$. It should be emphasized that the following examination of deformation is based on the assumption that CSL configuration tries to sustain through the deformation instances via slide of filaments. Such performance guarantees conical-helix configuration and in fact is realistic. Since only the origin (point "*O*" in Fig. 3) of disclination on either the center of a hexagon or an individual atom could give rise

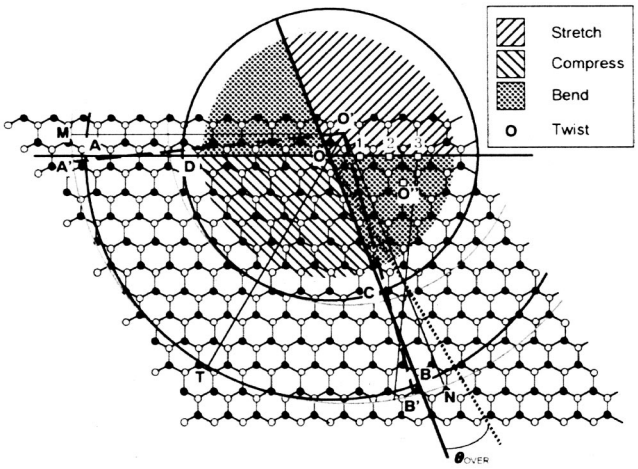

FIG. 3. Schematic presentation of deformation model for HCNT.

to CSLs,[36] deformation of HCNTs can simply be regarded as movement of the origin from one lattice point to another. Then we can define the regions where the origin will reach associated with different deformation processes (see Fig. 3). The directions of tensile stress are circumvented inside the same conical shape as indicated in Fig. 4(a). On the two-dimensional filamentary sheet (Fig. 3), the tensile stress will move the origin outwards to the area bounded by the extended lines from *AD* and *BC*. A stretching performance, for example, from point *O* to *O′* will increase the disclination radius (from *OA* to *O′T*). Provided that no twist is involved in the stretching, the number of wrapping layers keeps constant. Then the new disclination must bind a filamentary fragment with about the same area as *ABCD*. This restricts the modification of disclination angle, which has to increase, hence decrement of apex angles. The new disclination angle is defined by *O′A′* and *O′B′*, which cut *AD* and *BC* in such a way that the total overlap angle matches a certain CSL configuration. We can always obtain such an overlap angle as revealed by the high density of CLSs on the filamentary sheet,[27–32,36] though the CSL could not necessarily have one of the most stable configurations, i.e., larger CSLs may form. The standard disclination configuration with increased radius

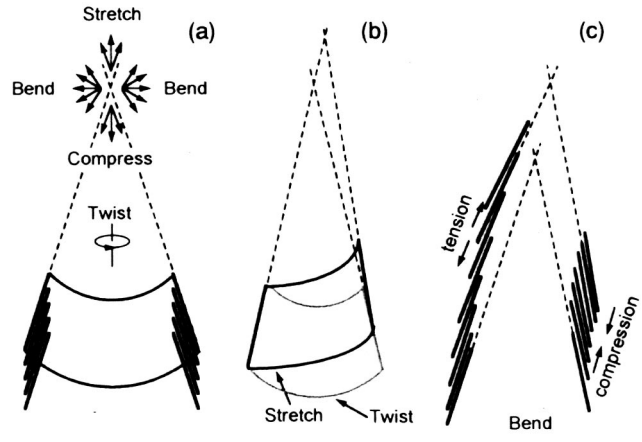

FIG. 4. Morphological modification upon different deformation processes: (a) before deformation, (b) after stretching or twisting, and (c) after bending.

($O'T$) exhibits decreased curvature (gray curves) compared to that prior to deformation. Then, winding of the original filamentary ribbon to form a new conical helix leads to climbing of the ribbon about the conical axis as shown in Fig. 4(b). The conical helix could be far from the symmetrical one and the helical steps increase. It can be seen that tension results in decrease in the overlapping area. The extreme of tension leads to an approximate cylindrical-spiral ribbon where parts of the neighboring layers may detach.

Similarly, the compressive stress will move the origin "O" inwards and make the apex angle increase and the nanotube short. Pure twisting neither moves the position of the origin nor changes the disclination radius, but simply modifies the disclination angles and apex angles. Since the number of monolayer sheets along the tube axis may increase by twisting in accordance with wrapping direction, or decrease for twisting in inverse direction, the length of the nanotubes either increases or decreases. For a deformation involving stretching or compressing in combination with twisting, the whole process could be dissociated into pure stretching or compressing, along with pure twisting about a new origin, or vice versa. Then, the geometry after deformation can easily be resolved.

During bending, the origin O moves into the regions outside that circumvented by the $360° - \theta_D$ angle. Since the connection line, e.g., through OO'', does not cross the original cone constituent ($ABCD$), it is impossible to define a new disclination configuration. Thus, in order to achieve the final conical configuration originated from O'', several monolayers with continuous modification of disclination must be involved. A possible deformation process is indicated in Fig. 3, displaying movement of the origin stepwise, i.e., $O \rightarrow 1 \rightarrow 2 \rightarrow 3$, and finally to O''. Therefore, at least four monolayers are involved during this bending performance. The number of monolayers that take part in the deformation is inverse proportional to the bending curvature. It can be seen from Fig. 3 that the first three steps are tensile and the last one is compressive. This is reasonable by noting that bending causes tension for the outer parts of the bending curvature while compression for the inner parts [see Fig. 4(c)]. Thereafter, bending can be regarded as the combination of successive tensile and compressive behaviors. During large-angle bending, numbers of conical monolayers take part in the deformation. Then, each monolayer only bears small distortion, which mitigates large strain of nanotubes. As a result, structural collapse is avoided, leading to high resistance to fracture for HCNT.

V. DISCUSSION

It has been seen from the above-given deformation models that stretching, compressing, bending, and twisting of HCNTs are all performed via simple rotation and/or slide of filaments. The nanotube keeps the rigid hexagon network and hollow conical-helix geometry, with a sole change in apex angles. A change in apex angle in the deformation process has been observed in Fig. 2. It should be noted here that irradiation induced deformation of HCNT displays unpredictable modification of tubule shape, which may include any of the above-given deformation processes. Anyhow, each of them changes the apex angle. The precise TEM study of the geometrical changes associated with each of deformation processes requires developments in experimental techniques, e.g., special specimen holder, so as to perform a subtle deformation on an individual nanotube.

The diffraction pattern in Fig. 2(h) demonstrates the structure of the HCNT prior to deformation. The entire region of the nanotube displays a uniform apex angle of 52°, which corresponds to the $180° + 21.8°$ disclination and a $\Sigma 7$ CSL.[27–29,36] After numerous deformation processes, the diffraction pattern [Fig. 2(i)] obtained from a short part of the nanotube which has almost retrieved the starting shape [Fig. 2(f)], exhibits reflection rings and circular streaks of (002) reflections, indicative of variation in apex angles. The apex angle is now peaked at ~35°, which refers to the disclination of $240° + 13.2°$, i.e., another stable helical-conical structure but with increased strain and larger CSL.[27–32,36] Then TEM image and diffraction pattern confirm reservation of HCH geometry and change of apex angle after deformation of the nanotube.

Based on a continuum elastic model, Tibbetts[37] and then Robertson *et al.*[38] derived that the strain energy of an individual atom in a curved filament should increase inversely proportional to the square of the radius of curvature, i.e., $\sigma_i = \lambda R_i^{-2}$, where R_i is the radius of curvature and λ is a constant determined by the elastic modulus, filamentary structure, and atomic size. The strain energy (σ) for a cone can then be regarded as the sum of σ_i for all atoms with a linear change of R_i, giving $\sigma = \Sigma\ \sigma_i = \Sigma\ \lambda R_i^{-2}$. It is seen that stretching or bending, as peculiar to the observed deformation in Fig. 2, leads to decrease in tubular radius and apex angles, hence increase in bending curvature and strain energy along with decrease in overlapping area. A stable HCNT configuration represents a status in which the overall strain energy does not surpass the total interlayer van der Waals interactions. The total interlayer interactions are dominated by the total overlapping area and CSLs. Thus for the present nanosized belt width, distorted configuration with increased strain and decreased overlapping area after electron-beam induced deformation must be unstable and will soon retrieve the previous stable geometry once the external stress is released. Then a spring-like mechanical behavior occurs. However in the present *in situ* TEM observation, the strong linking forces of the substrate foil prevent parts of the long nanotube from full recovery to the initial apex angle.

Stepwise changes in disclination configuration avoid disastrous failure of HCNTs owing to the fact that extra energies are absorbed to escape from the series of stable configurations. We must note that the *reversible* deformation of HCNTs does not require an introduction of topological defects like dislocation dipoles as in the case of carbon nanotubes. HCNTs keep the rigid structural configuration with a sole change in the apex angles. The outstanding room-temperature mechanical properties presently observed in a covalent compound are comparable to, and in some senses superior to, metals and polymers. The high thermal and chemical stability of BN will expedite its substitution for metal and polymer fibers in high performance composite materials where reinforcement by BN HCNTs can be taken into

effect at both low and high temperatures. It is clearly seen that the novel properties of a graphitic material are highly structure- and size-dependent, which only tubes with hollow conical-helix geometry can possess whereas the cylindrical nanotubes and nonhelical cones do not. It appears that a nano-scaled HCNT guarantees slide prior to cleavage or collapse. The specific geometry of HCNTs has taken advantage of both high stiffness and extraordinary flexibility of BN filaments, and easiness of interlayer slide, hence exhibiting high resistance to fracture.

VI. SUMMARY

We have observed a remarkable low-temperature elastic behavior of BN helical-conical nanotubes by an *in situ* transmission electron microscopy. The nanotubes can be bent by a maximum angle as high as 180° at room temperature and then retrieve the starting morphology without any evidence of structural failure. A theoretical model is established, which reveals a deformation dominated by rotation and/or slide of filaments with a sole change in apex angles. No topological defects have been introduced during the deformation and the rigid honeycomb filamentary structure and HCH geometry remain undestroyed after deformation. The low-temperature elastic property of the present HCNTs highlights their application in high-performance materials for both low- and high-temperature usages.

ACKNOWLEDGMENTS

We thank Dr. M. Mitome and K. Kurashima for assistance in experimental work.

[1] S. Iijima, Nature (London) **354**, 56 (1991).
[2] J. Despres, E. Daguerre, and K. Lafdi, Carbon **33**, 87 (1995).
[3] N. G. Chopra, L. Benedict, V. Crespi, M. L. Cohen, S. G. Louie, and A. Zettl, Nature (London) **377**, 135 (1995).
[4] R. Ruoff and D. Lorents, Bull. Am. Phys. Soc. **40**, 173 (1995).
[5] B. I. Yakobson, C. J. Brabec, and J. Bernholc, Phys. Rev. Lett. **76**, 2511 (1996).
[6] M. M. J. Treacy, T. W. Ebbesen, and J. M. Gibson, Nature (London) **381**, 678 (1996).
[7] E. W. Wong, P. E. Sheehan, and C. M. Lieber, Science **277**, 1971 (1997).
[8] E. Hernandez, C. Goze, P. Bernier, and A. Rubio, Phys. Rev. Lett. **80**, 4502 (1998).
[9] S. Iijima, C. Brabec, A. Maiti, and J. Bernholc, J. Chem. Phys. **104**, 2089 (1996).
[10] M. R. Falvo, G. J. Clary, R. M. Taylor II, V. Chi, F. P. Brooks, Jr., S. Washburn, and R. Superfine, Nature (London) **389**, 582 (1997).
[11] A. Krishnan, E. Dujardin, T. W. Ebbesen, P. N. Yanilos, and M. M. J. Treacy, Phys. Rev. B **58**, 14013 (1998).
[12] J. Muster, M. Burghard, S. Roth, G. S. Dusberg, E. Hernandez, and A. Rubio, J. Vac. Sci. Technol. B **16**, 2796 (1998).
[13] J. P. Salvetat, G. A. D. Briggs, J. M. Bonard, R. R. Bacsa, A. J. Kulik, T. Stockli, N. A. Burnham, and L. Forro, Phys. Rev. Lett. **82**, 944 (1999).
[14] L. Vaccarini, C. Goze, L. Henrard, E. Hernandez, P. Bernier, and A. Rubio, Carbon **38**, 1681 (2000).
[15] V. H. Crespi, M. L. Cohen, and A. Rubio, Phys. Rev. Lett. **79**, 2093 (1997).
[16] P. Zhang, P. E. Lammert, and V. H. Crespi, Phys. Rev. Lett. **81**, 5346 (1998).
[17] M. Buongiorno-Nardelli, B. I. Yakobson, and J. Nernholc, Phys. Rev. Lett. **81**, 4656 (1998).
[18] M. Buongiorno-Nardelli, B. I. Yakobson, and J. Nernholc, Phys. Rev. B **57**, 4277 (1998).
[19] N. G. Chopra, R. J. Luyken, K. Cherrey, V. H. Crespi, M. L. Cohen, S. G. Louie, and A. Zettl, Science **269**, 966 (1995).
[20] A. Loiseau, F. Willaime, N. Demoncy, G. Hug, and H. Pascard, Phys. Rev. Lett. **76**, 4737 (1996).
[21] D. Golberg, Y. Bando, M. Eremets, K. Takemura, K. Kurashima, and H. Yusa, Appl. Phys. Lett. **69**, 2045 (1996).
[22] *Synthesis and Properties of Boron Nitride*, edited by J. Pouch and A. Alterovitz (Materials Science Forum, Trans. Tech., Aedermannsdorf, Switzerland, 1999).
[23] N. G. Chopra and A. Zettl, Solid State Commun. **105**, 297 (1998).
[24] K. N. Kudin, G. E. Scuseria, and B. I. Yakobson, Phys. Rev. B **64**, 235406 (2001).
[25] H. F. Bettinger, T. Dumitrica, G. E. Scuseria, and B. I. Yakobson, Phys. Rev. B **65**, 041406 (2002).
[26] F. F. Xu, Y. Bando, R. Z. Ma, D. Golberg, Y. B. Li, and M. Mitome, J. Am. Chem. Soc. (in press).
[27] D. D. Double and A. Hellawell, Acta Metall. **22**, 481 (1974).
[28] S. Amelinckx, W. Luyten, T. Krekels, G. van Tendeloo, and J. van Landuyt, J. Cryst. Growth **121**, 543 (1992).
[29] A. Krishnan, E. Dujardin, M. M. J. Treacy, J. Hugdahl, S. Lynum, and T. W. Ebbesen, Nature (London) **388**, 451 (1997).
[30] L. Bourgeois, Y. Bando, S. Shinozaki, K. Kurashima, and T. Sato, Acta Crystallogr., Sect. A: Found. Crystallogr. **55**, 168 (1999).
[31] L. Bourgeois, Y. Bando, K. Kurashima, and T. Sato, Philos. Mag. A **80**, 129 (2000).
[32] L. Bourgeois, Y. Bando, W. Q. Han, and T. Sato, Phys. Rev. B **61**, 7686 (2000).
[33] W. H. Knechtel, G. S. Dusberg, W. J. Blau, E. Hernandez, and A. Rubio, Appl. Phys. Lett. **73**, 1961 (1998).
[34] M. R. Falvo, R. M. Taylor II, A. Helser, V. Chi, F. Pl Brooks, Jr., S. Washburn, and R. Superfine, Nature (London) **397**, 236 (1999).
[35] J. Cumings and A. Zettl, Science **289**, 602 (2000).
[36] F. F. Xu and Y. Bando, Acta Crystallogr., Sect. A: Found. Crystallogr. **59**, 168 (2003).
[37] G. G. Tibbetts, J. Cryst. Growth **66**, 632 (1984).
[38] D. H. Robertson, D. W. Brenner, and J. W. Mintmire, Phys. Rev. B **45**, 12592 (1992).